

IXPE observations of the quintessential wind-accreting X-ray pulsar Vela X-1

SOFIA V. FORSBLOM ¹ JURI POUTANEN ^{1,2} SERGEY S. TSYGANKOV ^{1,2} MATTEO BACHETTI ³
ALESSANDRO DI MARCO ⁴ VICTOR DOROSHENKO ⁵ JEREMY HEYL ⁶ FABIO LA MONACA ⁴
CHRISTIAN MALACARIA ⁷ HERMAN L. MARSHALL ⁸ FABIO MULERI ⁴ ALEXANDER A. MUSHTUKOV ^{9,10}
MAURA PILIA ³ DANIELE ROGANTINI ⁸ VALERY F. SULEIMANOV ⁵ ROBERTO TAVERNA ¹¹ FEI XIE ^{12,4}
IVÁN AGUDO ¹³ LUCIO A. ANTONELLI ^{14,15} LUCA BALDINI ^{16,17} WAYNE H. BAUMGARTNER ¹⁸
RONALDO BELLAZZINI ¹⁶ STEFANO BIANCHI ¹⁹ STEPHEN D. BONGIORNO ¹⁸ RAFFAELLA BONINO ^{20,21}
ALESSANDRO BREZ ¹⁶ NICCOLÒ BUCCIANTINI ^{22,23,24} FIAMMA CAPITANIO ⁴ SIMONE CASTELLANO ¹⁶
ELISABETTA CAVAZZUTI ²⁵ CHIEN-TING CHEN ²⁶ STEFANO CIPRINI ^{27,15} ENRICO COSTA ⁴
ALESSANDRA DE ROSA ⁴ ETTORE DEL MONTE ⁴ LAURA DI GESU ²⁵ NICCOLÒ DI LALLA ²⁸
IMMACOLATA DONNARUMMA ²⁵ MICHAL DOVČIAK ²⁹ STEVEN R. EHLERT ¹⁸ TERUAKI ENOTO ³⁰
YURI EVANGELISTA ⁴ SERGIO FABIANI ⁴ RICCARDO FERRAZZOLI ⁴ JAVIER A. GARCIA ³¹ SHUICHI GUNJI ³²
KIYOSHI HAYASHIDA ^{33,*} WATARU IWAKIRI ³⁴ SVETLANA G. JORSTAD ^{35,36} PHILIP KAARET ^{18,37}
VLADIMIR KARAS ²⁹ TAKAO KITAGUCHI ³⁰ JEFFERY J. KOLODZIEJCZAK ¹⁸ HENRIC KRAWCZYNSKI ³⁸
LUCA LATRONICO ²⁰ IOANNIS LIODAKIS ³⁹ SIMONE MALDERA ²⁰ ALBERTO MANFREDA ¹⁶ FRÉDÉRIC MARIN ⁴⁰
ANDREA MARINUCCI ²⁵ ALAN P. MARSCHER ³⁵ GIORGIO MATT ¹⁹ IKUYUKI MITSUISHI ⁴¹ TSUNEFUMI MIZUNO ⁴²
MICHELA NEGRO ^{43,44,45} CHI-YUNG NG ⁴⁶ STEPHEN L. O'DELL ¹⁸ NICOLA OMODEI ²⁸ CHIARA OPPEDISANO ²⁰
ALESSANDRO PAPITTO ¹⁴ GEORGE G. PAVLOV ⁴⁷ ABEL L. PEIRSON ²⁸ MATTEO PERRI ^{15,14}
MELISSA PESCE-ROLLINS ¹⁶ PIERRE-OLIVIER PETRUCCI ⁴⁸ ANDREA POSSENTI ³ SIMONETTA PUC CETTI ¹⁵
BRIAN D. RAMSEY ¹⁸ JOHN RANKIN ⁴ AJAY RATHEESH ⁴ OLIVER J. ROBERTS ²⁶ ROGER W. ROMANI ²⁸
CARMELO SGRÒ ¹⁶ PATRICK SLANE ⁴⁹ PAOLO SOFFITTA ⁴ GLORIA SPANDRE ¹⁶ RASHID A. SUNYAEV ^{50,2}
DOUG SWARTZ ²⁶ TORU TAMAGAWA ³⁰ FABRIZIO TAVECCHIO ⁵¹ YUZURU TAWARA ⁴¹ ALLYN F. TENNANT ¹⁸
NICHOLAS E. THOMAS ¹⁸ FRANCESCO TOMBESI ^{52,27,53} ALESSIO TROIS ³ ROBERTO TUROLLA ^{11,54}
JACCO VINK ⁵⁵ MARTIN C. WEISSKOPF ¹⁸ KINWAH WU ⁵⁴ AND SILVIA ZANE ⁵⁴

(IXPE COLLABORATION)

¹Department of Physics and Astronomy, FI-20014 University of Turku, Finland

²Space Research Institute of the Russian Academy of Sciences, Profsoyuznaya Str. 84/32, Moscow 117997, Russia

³INAF Osservatorio Astronomico di Cagliari, Via della Scienza 5, 09047 Selargius (CA), Italy

⁴INAF Istituto di Astrofisica e Planetologia Spaziali, Via del Fosso del Cavaliere 100, 00133 Roma, Italy

⁵Institut für Astronomie und Astrophysik, Universität Tübingen, Sand 1, D-72076 Tübingen, Germany

⁶Department of Physics and Astronomy, University of British Columbia, Vancouver, BC V6T 1Z1, Canada

⁷International Space Science Institute, Hallerstrasse 6, 3012 Bern, Switzerland

⁸MIT Kavli Institute for Astrophysics and Space Research, Massachusetts Institute of Technology, 77 Massachusetts Avenue, Cambridge, MA 02139, USA

⁹Astrophysics, Department of Physics, University of Oxford, Denys Wilkinson Building, Keble Road, Oxford OX1 3RH, UK

¹⁰Leiden Observatory, Leiden University, NL-2300RA Leiden, The Netherlands

¹¹Dipartimento di Fisica e Astronomia, Università degli Studi di Padova, Via Marzolo 8, 35131 Padova, Italy

¹²Guangxi Key Laboratory for Relativistic Astrophysics, School of Physical Science and Technology, Guangxi University, Nanning 530004, China

¹³Instituto de Astrofísica de Andalucía – CSIC, Glorieta de la Astronomía s/n, 18008 Granada, Spain

¹⁴INAF Osservatorio Astronomico di Roma, Via Frascati 33, 00040 Monte Porzio Catone (RM), Italy

¹⁵Space Science Data Center, Agenzia Spaziale Italiana, Via del Politecnico snc, 00133 Roma, Italy

¹⁶Istituto Nazionale di Fisica Nucleare, Sezione di Pisa, Largo B. Pontecorvo 3, 56127 Pisa, Italy

¹⁷Dipartimento di Fisica, Università di Pisa, Largo B. Pontecorvo 3, 56127 Pisa, Italy

¹⁸NASA Marshall Space Flight Center, Huntsville, AL 35812, USA

- ¹⁹ *Dipartimento di Matematica e Fisica, Università degli Studi Roma Tre, Via della Vasca Navale 84, 00146 Roma, Italy*
- ²⁰ *Istituto Nazionale di Fisica Nucleare, Sezione di Torino, Via Pietro Giuria 1, 10125 Torino, Italy*
- ²¹ *Dipartimento di Fisica, Università degli Studi di Torino, Via Pietro Giuria 1, 10125 Torino, Italy*
- ²² *INAF Osservatorio Astrofisico di Arcetri, Largo Enrico Fermi 5, 50125 Firenze, Italy*
- ²³ *Dipartimento di Fisica e Astronomia, Università degli Studi di Firenze, Via Sansone 1, 50019 Sesto Fiorentino (FI), Italy*
- ²⁴ *Istituto Nazionale di Fisica Nucleare, Sezione di Firenze, Via Sansone 1, 50019 Sesto Fiorentino (FI), Italy*
- ²⁵ *Agenzia Spaziale Italiana, Via del Politecnico snc, 00133 Roma, Italy*
- ²⁶ *Science and Technology Institute, Universities Space Research Association, Huntsville, AL 35805, USA*
- ²⁷ *Istituto Nazionale di Fisica Nucleare, Sezione di Roma “Tor Vergata”, Via della Ricerca Scientifica 1, 00133 Roma, Italy*
- ²⁸ *Department of Physics and Kavli Institute for Particle Astrophysics and Cosmology, Stanford University, Stanford, California 94305, USA*
- ²⁹ *Astronomical Institute of the Czech Academy of Sciences, Boční II 1401/1, 14100 Praha 4, Czech Republic*
- ³⁰ *RIKEN Cluster for Pioneering Research, 2-1 Hirosawa, Wako, Saitama 351-0198, Japan*
- ³¹ *California Institute of Technology, Pasadena, CA 91125, USA*
- ³² *Yamagata University, 1-4-12 Kojirakawa-machi, Yamagata-shi 990-8560, Japan*
- ³³ *Osaka University, 1-1 Yamadaoka, Suita, Osaka 565-0871, Japan*
- ³⁴ *International Center for Hadron Astrophysics, Chiba University, Chiba 263-8522, Japan*
- ³⁵ *Institute for Astrophysical Research, Boston University, 725 Commonwealth Avenue, Boston, MA 02215, USA*
- ³⁶ *Department of Astrophysics, St. Petersburg State University, Universitetsky pr. 28, Petrodvoretz, 198504 St. Petersburg, Russia*
- ³⁷ *Department of Physics and Astronomy, University of Iowa, Iowa City, IA 52242, USA*
- ³⁸ *Physics Department and McDonnell Center for the Space Sciences, Washington University in St. Louis, St. Louis, MO 63130, USA*
- ³⁹ *Finnish Centre for Astronomy with ESO, 20014 University of Turku, Finland*
- ⁴⁰ *Université de Strasbourg, CNRS, Observatoire Astronomique de Strasbourg, UMR 7550, 67000 Strasbourg, France*
- ⁴¹ *Graduate School of Science, Division of Particle and Astrophysical Science, Nagoya University, Furo-cho, Chikusa-ku, Nagoya, Aichi 464-8602, Japan*
- ⁴² *Hiroshima Astrophysical Science Center, Hiroshima University, 1-3-1 Kagamiyama, Higashi-Hiroshima, Hiroshima 739-8526, Japan*
- ⁴³ *University of Maryland, Baltimore County, Baltimore, MD 21250, USA*
- ⁴⁴ *NASA Goddard Space Flight Center, Greenbelt, MD 20771, USA*
- ⁴⁵ *Center for Research and Exploration in Space Science and Technology, NASA/GSFC, Greenbelt, MD 20771, USA*
- ⁴⁶ *Department of Physics, University of Hong Kong, Pokfulam, Hong Kong*
- ⁴⁷ *Department of Astronomy and Astrophysics, Pennsylvania State University, University Park, PA 16801, USA*
- ⁴⁸ *Université Grenoble Alpes, CNRS, IPAG, 38000 Grenoble, France*
- ⁴⁹ *Center for Astrophysics, Harvard & Smithsonian, 60 Garden St, Cambridge, MA 02138, USA*
- ⁵⁰ *Max Planck Institute for Astrophysics, Karl-Schwarzschild-Str 1, D-85741 Garching, Germany*
- ⁵¹ *INAF Osservatorio Astronomico di Brera, via E. Bianchi 46, 23807 Merate (LC), Italy*
- ⁵² *Dipartimento di Fisica, Università degli Studi di Roma “Tor Vergata”, Via della Ricerca Scientifica 1, 00133 Roma, Italy*
- ⁵³ *Department of Astronomy, University of Maryland, College Park, Maryland 20742, USA*
- ⁵⁴ *Mullard Space Science Laboratory, University College London, Holmbury St Mary, Dorking, Surrey RH5 6NT, UK*
- ⁵⁵ *Anton Pannekoek Institute for Astronomy & GRAPPA, University of Amsterdam, Science Park 904, 1098 XH Amsterdam, The Netherlands*

ABSTRACT

The radiation from accreting X-ray pulsars was expected to be highly polarized, with some estimates for the polarization degree of up to 80%. However, phase-resolved and energy-resolved polarimetry of X-ray pulsars is required in order to test different models and to shed light on the emission processes and the geometry of the emission region. Here we present the first results of the observations of the accreting X-ray pulsar Vela X-1 performed with the *Imaging X-ray Polarimetry Explorer* (IXPE). Vela X-1 is considered to be the archetypal example of a wind-accreting high-mass X-ray binary system, consisting of a highly magnetized neutron star accreting matter from its supergiant stellar companion. The spectro-polarimetric analysis of the phase-averaged data for Vela X-1 reveals a polarization degree (PD) of $2.3 \pm 0.4\%$ at the polarization angle (PA) of $-47.3 \pm 5.4^\circ$. A low PD is consistent with the results obtained for other X-ray pulsars and is likely related to the inverse temperature structure of the neutron star atmosphere. The energy-resolved analysis shows the PD above 5 keV reaching 6–10%, and a $\sim 90^\circ$ difference in the PA compared to the data in the 2–3 keV range. The phase-resolved spectro-polarimetric analysis finds a PD in the range 0–9% with the PA varying between -80° and 40° .

Keywords: accretion – magnetic fields – pulsars: individual: Vela X-1 – stars: neutron – X-rays: binaries

1. INTRODUCTION

Accreting X-ray pulsars (XRP) harbor some of the strongest magnetic fields in the entire Universe, which can be as large as several times 10^{12} G. The strong magnetic field channels accreting matter onto the polar regions at the neutron star surface, where it produces hot-spots that are bright in the X-rays; these spots rotate in and out of the observer’s line-of-sight, resulting in the appearance of pulsed X-ray emission. Highly magnetized XRP represent unique laboratories and much information is embedded in the interplay between the immense magnetic fields and the accretion flow. Observations of emission from accreting XRP therefore constitute a substantial area of interest for theoretical models of matter interactions with ultrastrong magnetic fields, which cannot be replicated in terrestrial laboratories (see [Mushtukov & Tsygankov 2022](#), for a recent review).

The magnetic field of the neutron star is the main cause for the polarized X-ray emission from accreting XRP. The scattering of photons in a highly magnetized plasma is expected to result in a large degree of polarization of the emerging X-ray emission, up to 80% ([Meszaros et al. 1988](#); [Caiazzo & Heyl 2021](#)). [Meszaros et al. \(1988\)](#) showed that linear X-ray polarization is strongly dependent on the geometry of the emission region, and also that it varies with energy and pulse phase. X-ray polarimetric observations of accreting XRP can therefore be used to probe the geometry of the emission region. The phase-resolved polarimetry can be used as a tool to constrain the viewing geometry and to distinguish between the models of their radiation.

A large window of opportunity to achieve significant observations of polarized X-ray emission opened up recently, thanks to the launch of the *Imaging X-ray Polarimetry Explorer* (IXPE, [Weisskopf et al. 2022](#)). IXPE is the first imaging X-ray polarimetric mission. For observations of XRP, the strategy is to detect pulsations in the polarized emission, as well as to measure the polarization degree (PD) and polarization angle (PA) as a function of the pulse phase, which allows for the system geometry to be determined.

Vela X-1 (associated with the Uhuru source 4U 0900–40) is a high-mass X-ray binary (HMXB) discovered as one of the first X-ray sources at the early years of X-

ray astronomy ([Chodil et al. 1967](#)) and remains one of the best studied objects among neutron star HMXBs. It is one of the brightest, persistent XRP chosen to be observed by IXPE. Vela X-1, located at a distance of about 2 kpc ([Kretschmar et al. 2021](#)), is often considered the quintessential wind accretor. It displays strong X-ray pulsations with a pulse period of 283 s ([McClinck et al. 1976](#)), variations with the orbital period of 8.964 days ([Ulmer et al. 1972](#); [van Kerkwijk et al. 1995](#)), and eclipses lasting for about two days per orbit. The lower limit on the orbital inclination was obtained at $i = 73^\circ$ ([van Kerkwijk et al. 1995](#)).

Persistent wind-accreting XRP are expected to have a different emission region geometry as opposed to the disk-accreting Be/X-ray binaries. Additionally, polarization signatures are expected to be introduced by the scattering in the dense asymmetric wind. The main goal is therefore to study the accretion geometry for wind-accretion and the properties of the dense stellar wind.

[Quaintrell et al. \(2003\)](#) have shown that the separation between the neutron star and its stellar companion, the B0.5Ib supergiant HD 77581 (also known as GP Vel), is only about 1.7 stellar radii and therefore the neutron star is deeply embedded in the stellar wind of its companion star. The stellar companion has a mass loss rate of $\sim 10^{-6} M_\odot \text{ yr}^{-1}$ ([Nagase et al. 1986](#)). The average X-ray luminosity of the source is $\sim 4 \times 10^{36} \text{ erg s}^{-1}$. The luminosity is, however, strongly variable on all time-scales, varying up to a factor of at least 20–30 ([Staubert et al. 2004](#); [Kreykenbohm et al. 2008](#)).

Observations of the cyclotron resonance scattering features (CRSFs) in the spectra of XRP provide a direct measurement of the magnetic field strength in the line-forming region. These features were first discovered in Vela X-1 by [Kendziorra et al. \(1992\)](#) by utilizing MirHEXE data, reporting a fundamental line around 25 keV and a first harmonic close to 50 keV. Evidence for these features was also given by [Makishima & Mihara \(1992\)](#) and they were further detailed by [Kretschmar et al. \(1996\)](#). Early observations with RXTE also confirmed this detection ([Kretschmar et al. 1997](#)). More recent observations of Vela X-1 by NuSTAR clearly detected the fundamental line at 25 keV together with a more prominent first harmonic at 55 keV and revealed a positive correlation between the harmonic line energy and the observed flux ([Fürst et al. 2014](#)). [La Parola et al. \(2016\)](#) confirmed a flux dependence of the first harmonic line energy and discovered its secular variation with time

* Deceased

Table 1. Orbital parameters for Vela X-1 adopted from the Fermi Gamma Ray Burst Monitor project (dated 2021 January 30).

Parameter	Value	Unit
Orbital period	8.9642140	d
$T_{\pi/2}$	2459115.02085	JED
$a_X \sin i$	113.105	light-sec
Longitude of periastron	162.33	deg
Eccentricity	0.0872	
Eclipse egress	0.12	
Eclipse ingress	0.92	

in the long-term data collected by Swift/BAT (see also Ji et al. 2019).

In this paper, we present the first results of X-ray polarimetric observations of Vela X-1 by IXPE carried out on two separate occasions during 2022. In Sect. 2, the data used in the paper are described. Sect. 3 is devoted to the description of the results: the analysis of the phase-averaged, phase-resolved, and energy-resolved polarimetric data are given. Finally, the discussion and a short summary are presented in Sect. 4.

2. DATA

IXPE is an observatory launched on December 9, 2021, as a NASA mission in partnership with the Italian space agency (ASI). IXPE consists of three telescope-detector systems which provide imaging polarimetry over a nominal 2–8 keV band at $\sim 30''$ angular resolution (half-power diameter). Each one of the three grazing incidence telescopes is comprised of a mirror module assembly (MMA), that focuses the X-rays onto a corresponding focal plane polarization-sensitive gas pixel electron tracking detector unit (DU). The detection principle is based on the photoelectric effect. All characteristics of each detected photon (sky coordinates, time of arrival, energy, and direction of the photo-electron) are measured simultaneously. A comprehensive description of the observatory, the instruments, and their performance is given by Soffitta et al. (2021) and Weisskopf et al. (2022).

IXPE observations of Vela X-1 were carried out between 2022 April 15–21 and November 30 – December 6, with the total effective exposure of $\simeq 280$ ks and $\simeq 270$ ks, respectively. The data have been processed with the IXPEOBSSIM package version 30.2.1 (Baldini et al. 2022) using the CalDB released on November 17, 2022. The position offset correction and energy calibration were applied before the scientific analysis of the data. Source photons were collected using a circular region with a radius $R_{\text{src}} = 70''$. The background region was chosen in

the form of an annulus with inner and outer radii equal to $2R_{\text{src}}$ and $4R_{\text{src}}$, respectively. Data from the first observation were cleaned from events due to solar events, which have been identified by comparing the IXPE light curve with the one from the Geostationary Operational Environmental Satellite (GOES), then removing time intervals where the IXPE count rate in the background annular region was higher than the mean background value plus three times the RMS of this count rate. The background makes up $\sim 3.6\%$ and $\sim 2.2\%$ of the total count rate of the source region in the 2–8 keV energy range for the first and second observation, respectively.

The `barycorr` tool from the `FTOOLS` package was used to correct the event arrival times to the barycenter of the Solar System. This was followed by a correction of arrival times as it relates to the effects of binary motion using the orbital parameters obtained by the *Fermi* Gamma Ray Burst Monitor¹ for Vela X-1 and given in Table 1.

Stokes I energy spectra have been binned to have at least 30 counts per energy channel, and the same energy binning was applied to the energy spectra of Stokes parameters Q and U . The energy spectra were fitted in the XSPEC package (Arnaud 1996) using χ^2 statistics, using the version 12 instrument response functions. The reported uncertainties are at the 68.3% confidence level (1σ), unless stated otherwise.

3. RESULTS

3.1. Light curve and pulse profile

The light curves from the first and second observation of Vela X-1 in the 2–8 keV energy range obtained with the IXPE observatory are shown in Figure 1. For the first observation of Vela X-1, the observing window can be separated into three parts: pre-eclipse (MJD 59684.7–59687.7), eclipse (MJD 59687.7–59689.5), and post-eclipse (MJD 59689.5–59690.5). The post-eclipse count rate of the source was about one order of magnitude greater than the pre-eclipse source count rate. During the eclipse, which lasted about two days, the count rate dropped by an order of magnitude compared to the pre-eclipse value. For the following analysis, only pre- and post-eclipse data were included, i.e., only data outside of the eclipse.

A spin period of $P_{\text{spin}} = 283.488(7)$ s and $P_{\text{spin}} = 283.437(6)$ s were measured for Vela X-1 for the first and second observation, respectively, using phase connection technique. The pulsed fraction in the 2–8 energy band, defined as $PF = (F_{\text{max}} - F_{\text{min}})/(F_{\text{max}} + F_{\text{min}})$ where

¹ <https://gammaray.nsstc.nasa.gov/gbm/science/pulsars.html>

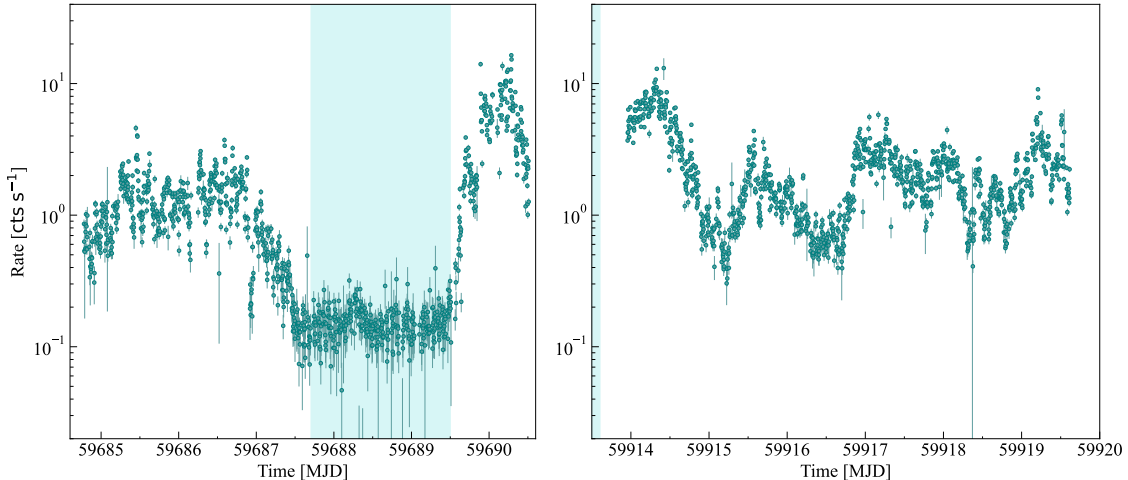


Figure 1. Background-corrected light curves of Vela X-1 in the 2–8 keV energy bands summed over the three DUs of IXPE for the first and second observation, shown in the left and right panels, respectively. The light curve time bin value was set to ~ 250 s. The time of the eclipse is marked by the blue-shaded area.

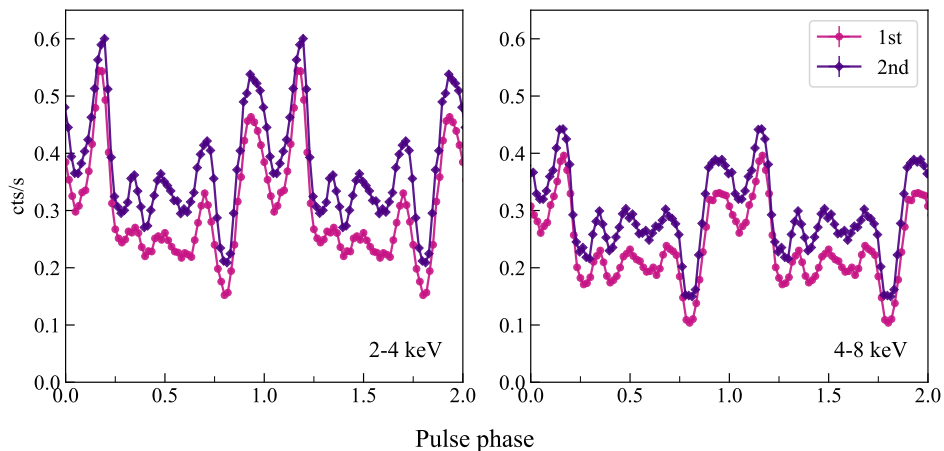


Figure 2. Pulse profiles of Vela X-1 as seen by IXPE in two different energy bands for the first and second observations, combined for DU1–3.

F_{\max} and F_{\min} are the maximum and minimum count rates in the pulse profile, respectively, was determined as $PF = 53.3 \pm 0.7\%$ for the first observation and as $PF = 48.1 \pm 0.9\%$ for the second observation. The resulting pulse profiles for Vela X-1 in two separate energy bands are shown in Figure 2.

3.2. Polarimetric analysis

First, the analysis of the polarimetric properties of Vela X-1 was carried out by using the PCUBE algorithm (xpbins tool) in the IXPEOBSSIM package, which is implemented according to the formalism by Kislak et al. (2015). The unweighted analysis has been used. We compute the normalized Stokes parameters, $q = Q/I$ and $u = U/I$, and the polarization degree using the formula $PD = \sqrt{q^2 + u^2}$ and ignoring the bias at low

Table 2. Measurements of the normalized Stokes parameters q and u , PD, and PA for the phase-averaged data of Vela X-1 in different energy bins using the PCUBE algorithm for the combined data set.

Energy (keV)	q (%)	u (%)	PD (%)	PA (deg)
2–3	0.5 ± 1.2	3.8 ± 1.2	3.9 ± 1.2	41.4 ± 9.1
3–4	0.2 ± 0.8	-1.4 ± 0.8	1.4 ± 0.8	-40.7 ± 16.1
4–5	-0.1 ± 0.8	-2.7 ± 0.8	2.7 ± 0.8	-46.4 ± 8.8
5–6	-1.2 ± 1.0	-5.6 ± 1.0	5.7 ± 1.0	-50.9 ± 4.8
6–7	-0.3 ± 1.2	-4.1 ± 1.2	4.1 ± 1.2	-47.3 ± 8.3
7–8	-2.7 ± 2.0	-9.4 ± 2.0	9.7 ± 2.0	-53.1 ± 6.0
2–8	-0.6 ± 0.5	-3.7 ± 0.5	3.7 ± 0.5	-49.9 ± 4.1

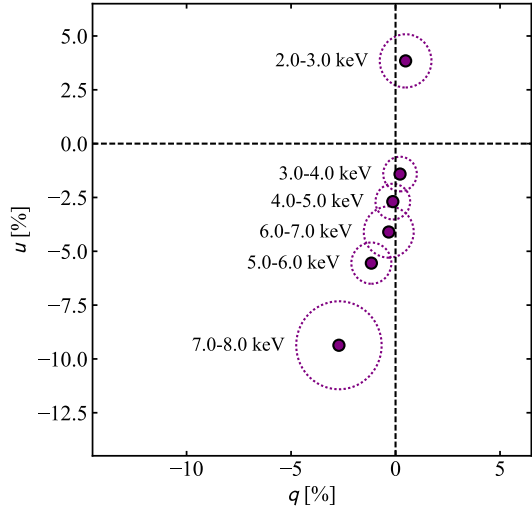


Figure 3. Energy dependence of the normalized Stokes parameters q and u for the phase-averaged data of the combined data set, obtained with the PCUBE algorithm.

signal-to-noise ratios (Serkowski 1958; Simmons & Stewart 1985; Maier et al. 2014; Mikhalev 2018) and the $PA = \frac{1}{2} \arctan(u/q)$ (measured counterclockwise on the sky from north to east).

In the entire IXPE energy band (2–8 keV), the average PD and PA are found to be $3.9 \pm 0.9\%$ and -51.5 ± 6.5 , respectively, for the first observation. For the second observation, the average PD and PA are found to be $3.7 \pm 0.7\%$ and -48.9 ± 5.2 , respectively.

Considering the similarities between the first and second observations, the data were combined into one single set of data in order to increase the statistics and further study the polarization properties of Vela X-1. In order to correctly phase-tag each event, the phase difference between the pulse profiles from the first and second observations was determined from cross-correlation (using the implementation provided by the Python library NumPy). Using the PCUBE algorithm (xpbins tool) in the IXPEOBSSIM package, the average PD and PA are found to be $3.7 \pm 0.5\%$ and -49.9 ± 4.1 , respectively, in the entire IXPE energy band.

We then studied the energy dependence of polarization by dividing the data into six energy bins. The PD is above the minimum detectable polarization at a 99% confidence level, MDP_{99} (Weisskopf et al. 2010), in all of the energy bins, except for the 3–4 keV bin, where the PD is below the MDP_{99} and in this case, the PA is not well constrained (Table 2 and Figure 3). The energy-resolved analysis shows that at higher energies (above 5 keV) the PD reaches 6–10% with the PA differing by $\sim 90^\circ$ from that below 3 keV.

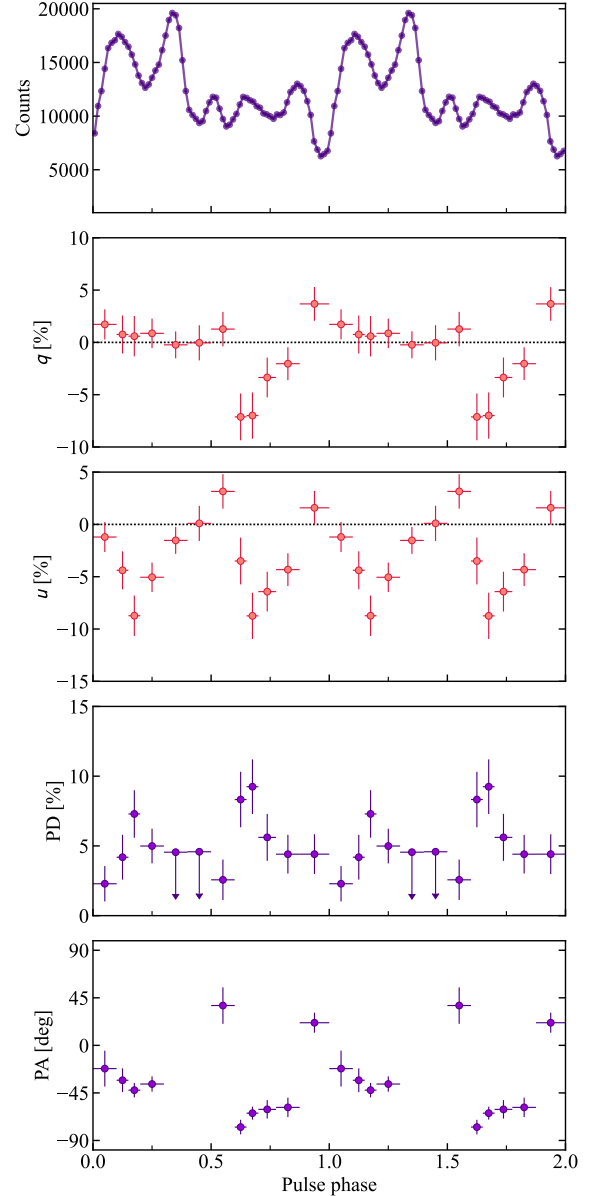


Figure 4. Phase-resolved analysis of Vela X-1 for the combined data set in the 2–7 keV range, combining data from all DUs. (a) Pulse profile. Panels (b) and (c) display the dependence of the Stokes q and u parameters, respectively, on the pulse phase, obtained for the phase-resolved polarimetric analysis utilizing the PCUBE algorithm. Panels (d) and (e) show the dependence of the PD and PA, respectively, on the pulse phase, obtained from the phase-resolved spectropolarimetric analysis using XSPEC. Upper limits (arrows) to the PD are at 99.73% (3σ) confidence level and are computed using a χ^2 with one degree of freedom.

Next, a phase-resolved polarimetric analysis was performed utilizing the PCUBE-algorithm. The results in the 2–7 keV energy band are given in Table 3 and are shown in Figure 4 for the combined data set.

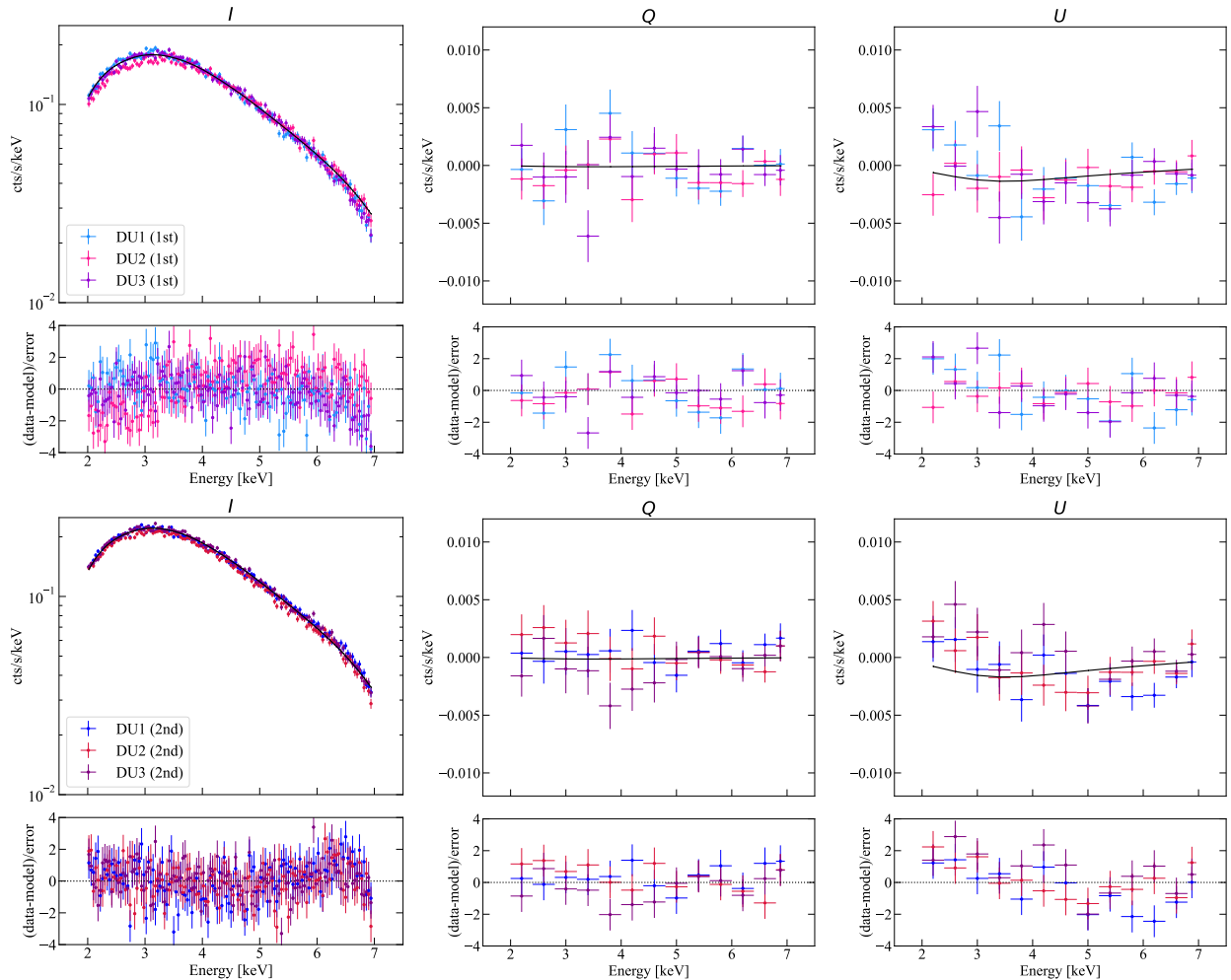


Figure 5. Stokes I , Q , and U energy distributions for the combined data set of Vela X-1 with the best-fit model superimposed for IXPE’s DUs (upper panels). The residuals between the best-fit model and the data are shown in the lower panels. Upper and lower plots correspond to the first and second observations, respectively, and are shown separately for clarity.

Then, the spectro-polarimetric analysis was performed according to the following steps. Source I , Q , and U Stokes spectra were produced via the `xpbin` tool’s `PHA1`, `PHA1Q`, and `PHA1U` algorithms, producing a full data set comprised of nine spectra per observation, three for each DU. As the background region is dominated by source events, background subtraction is not applied (Di Marco et al. 2023). Here we also used unweighted analysis. The `XSPEC` package (version 12.12.1) (Arnaud 1996), which is a part of the standard high-energy astrophysics software suite `HEASOFT`, was used to study polarization as a function of energy. All 18 spectra were fitted simultaneously in `XSPEC`.

There are several phenomenological spectral models used to describe the spectral continuum of Vela X-1. However, it is well known that except for a soft excess below 3 keV, the X-ray emission below 10 keV can be well described by a simple absorbed power law with an iron line at 6.4 keV. Due to the restricted energy range

covered by IXPE and the energy resolution of the instrument (Weisskopf et al. 2022), we used a simple model consisting of a power law affected by interstellar absorption (model `tbabs` with the abundances from Wilms et al. 2000) combined with the `polconst` polarization model, which assumes energy-independent PD and PA. In order to account for the soft excess below 3 keV, a partial covering fraction absorption (model `tbpcf`) was introduced as well, which applies an added column density to a fraction of the power law. The re-normalization constant, `const`, was used to account for the possibility of discrepancies between the different DUs, and for DU1 it was fixed to unity. The final model

$$\text{tbabs} \times \text{tbpcf} \times \text{polconst} \times \text{powerlaw} \times \text{const}$$

was subsequently applied to both the phase-averaged and phase-resolved data. The spectral analysis was confined to the 2–7 keV energy band, ignoring photons above 7 keV due to remaining calibration uncertainties.

Table 3. Pulse phase dependence of the normalized Stokes q and u parameters for the combined data set from the polarimetric analysis (2–7 keV) using the PCUBE algorithm and the spectral parameters, PD and PA obtained by the spectro-polarimetric analysis. An upper limit to the PD at 99.73% (3σ) confidence level is computed using a χ^2 with one degree of freedom.

Phase	q (%)	u (%)	N_{H} (10^{22} cm^{-2})	$N_{\text{H,tbpcf}}$ (10^{22} cm^{-2})	f_{cov}	Photon index	PD (%)	PA (deg)	$\chi^2/\text{d.o.f.}$
0.000–0.100	1.7 ± 1.4	-1.2 ± 1.4	$6.0^{+0.7}_{-0.8}$	$23.0^{+1.8}_{-2.2}$	0.82 ± 0.02	$1.55^{+0.13}_{-0.16}$	2.3 ± 1.2	-22.0 ± 16.9	2160/2152
0.100–0.150	0.8 ± 1.8	-4.4 ± 1.8	$4.4^{+1.0}_{-1.4}$	$18.5^{+2.1}_{-2.0}$	$0.83^{+0.04}_{-0.03}$	1.26 ± 0.16	4.2 ± 1.6	-33.0 ± 11.3	2162/2029
0.150–0.200	0.6 ± 1.9	-8.7 ± 1.9	$4.9^{+1.2}_{-2.1}$	$18.4^{+3.2}_{-3.4}$	$0.77^{+0.07}_{-0.04}$	$0.96^{+0.19}_{-0.22}$	7.3 ± 1.7	-42.4 ± 6.8	2081/2011
0.200–0.300	0.9 ± 1.4	-5.1 ± 1.4	$3.8^{+0.8}_{-0.9}$	$19.9^{+2.1}_{-1.9}$	0.80 ± 0.02	$0.75^{+0.14}_{-0.13}$	5.0 ± 1.2	-36.6 ± 7.2	2284/2179
0.300–0.400	-0.2 ± 1.3	-1.5 ± 1.3	$4.0^{+0.9}_{-1.1}$	$16.5^{+1.7}_{-1.4}$	$0.81^{+0.04}_{-0.03}$	1.11 ± 0.11	< 4.6	—	2304/2185
0.400–0.500	0.0 ± 1.7	0.1 ± 1.7	$4.2^{+0.8}_{-1.2}$	$20.5^{+2.5}_{-2.9}$	0.78 ± 0.03	1.08 ± 0.2	< 4.6	—	2057/2086
0.500–0.600	1.3 ± 1.6	3.2 ± 1.6	$2.1^{+0.9}_{-1.2}$	$17.7^{+1.7}_{-1.7}$	0.83 ± 0.03	0.63 ± 0.13	2.6 ± 1.5	37.7 ± 17.2	2230/2116
0.600–0.650	-7.1 ± 2.2	-3.5 ± 2.2	$3.8^{+1.0}_{-1.5}$	$21.3^{+2.6}_{-3.0}$	0.82 ± 0.03	$0.98^{+0.19}_{-0.22}$	8.3 ± 2.0	-77.3 ± 6.9	1885/1858
0.650–0.700	-7.0 ± 2.2	-8.7 ± 2.2	$2.5^{+1.2}_{-1.8}$	$18.2^{+2.4}_{-2.1}$	0.84 ± 0.04	0.73 ± 0.18	9.2 ± 2.0	-64.2 ± 6.1	1934/1912
0.700–0.775	-3.4 ± 1.9	-6.4 ± 1.9	$0.6^{+1.5}_{-0.6}$	$15.3^{+2.0}_{-1.2}$	$0.85^{+0.02}_{-0.05}$	$0.30^{+0.15}_{-0.13}$	5.6 ± 1.6	-60.6 ± 8.7	2025/2038
0.775–0.875	-2.0 ± 1.6	-4.3 ± 1.6	$4.0^{+0.7}_{-1.0}$	$20.6^{+2.0}_{-2.2}$	0.81 ± 0.02	$1.05^{+0.14}_{-0.15}$	4.4 ± 1.4	-58.7 ± 9.2	2117/2134
0.875–1.000	3.7 ± 1.6	1.6 ± 1.6	$3.1^{+1.2}_{-2.1}$	$14.9^{+1.9}_{-1.7}$	$0.81^{+0.07}_{-0.05}$	$0.95^{+0.13}_{-0.15}$	4.4 ± 1.4	21.4 ± 9.5	2271/2092

Table 4. Spectral parameters for the best-fit model obtained from the phase-averaged spectro-polarimetric analysis of the combined data set.

Parameter	Value	Unit
N_{H}	3.8 ± 0.3	10^{22} cm^{-2}
$N_{\text{H,tbpcf}}$	$18.5^{+0.7}_{-0.6}$	10^{22} cm^{-2}
f_{cov}	0.80 ± 0.01	
$\text{const}_{\text{DU}2}$	0.964 ± 0.003	
$\text{const}_{\text{DU}3}$	0.923 ± 0.002	
Photon index	0.93 ± 0.04	
PD	2.3 ± 0.4	%
PA	-47.3 ± 5.4	deg
$\text{Flux}_{2-8 \text{ keV}}$	$7.93^{+0.02}_{-0.06}$	$10^{-10} \text{ erg cm}^{-2} \text{ s}^{-1}$
$\text{Luminosity}_{2-8 \text{ keV}}$	3.8×10^{35}	$\text{erg s}^{-1} \text{ at } d = 2.0 \text{ kpc}$
χ^2 (d.o.f.)	2640.19 (2222)	

For the phase-averaged data, the results of the spectral fitting, including the best-fit model, are shown in Figure 5 and the best-fit model parameters are found in Table 4. The `steppar` command in XSPEC was used to create the confidence contours for the polarization measurements, and the resulting contour plots at 68.3%, 95.45% and 99.73% confidence levels are presented in Figure 6. The results of the phase-averaged polarimetric analysis for the two different approaches give compatible results.

A wavy structure of the Stokes U parameter residuals in Figure 5 (see also Fig. 3) indicates that polarization is energy dependent. Thus, we replaced the `polconst` polarization model with the `pollin` model, corresponding to a linear energy dependence of the PD and PA. We as-

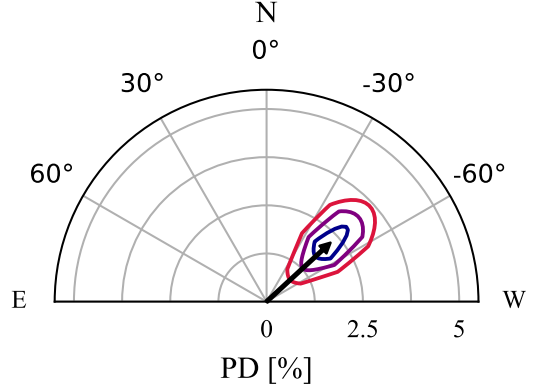


Figure 6. Polarization vector of Vela X-1 from the results of the phase-averaged spectro-polarimetric analysis of the combined data set. Contours at 68.3%, 95.45% and 99.73% confidence, are shown in blue, purple, and red, respectively.

sumed an energy-independent PA (ψ_1 in XSPEC; we fixed $\psi_{\text{slope}} = 0$), and allowed the PD to vary with photon energy E (keV) as $\text{PD}(E) = A_1 + A_{\text{slope}}(E - 1)$. This results in an improved fit ($\chi^2/\text{d.o.f.} = 2608.51/2221$ with an F-test probability of 2.3×10^{-7}). The best-fit parameters are $A_1 = -5.3 \pm 2.3\%$ and $A_{\text{slope}} = 2.2 \pm 0.6\%$, and $\text{PA} = \psi_1 = -47.3 \pm 5.4$. The negative A_1 means that the PA at lower energies is rotated by 90° relative to the PA at higher energies and the PD is zero at ≈ 3.4 keV. Such a model is able to describe the observed behavior of Stokes Q and U parameters in Figures 3 and 5.

For the phase-resolved spectro-polarimetric analysis, I , Q , and U Stokes spectra were extracted for each phase bin individually, again utilizing the `xpbin` tool's `PHA1`, `PHA1Q`, and `PHA1U` algorithms. The I , Q , and U Stokes

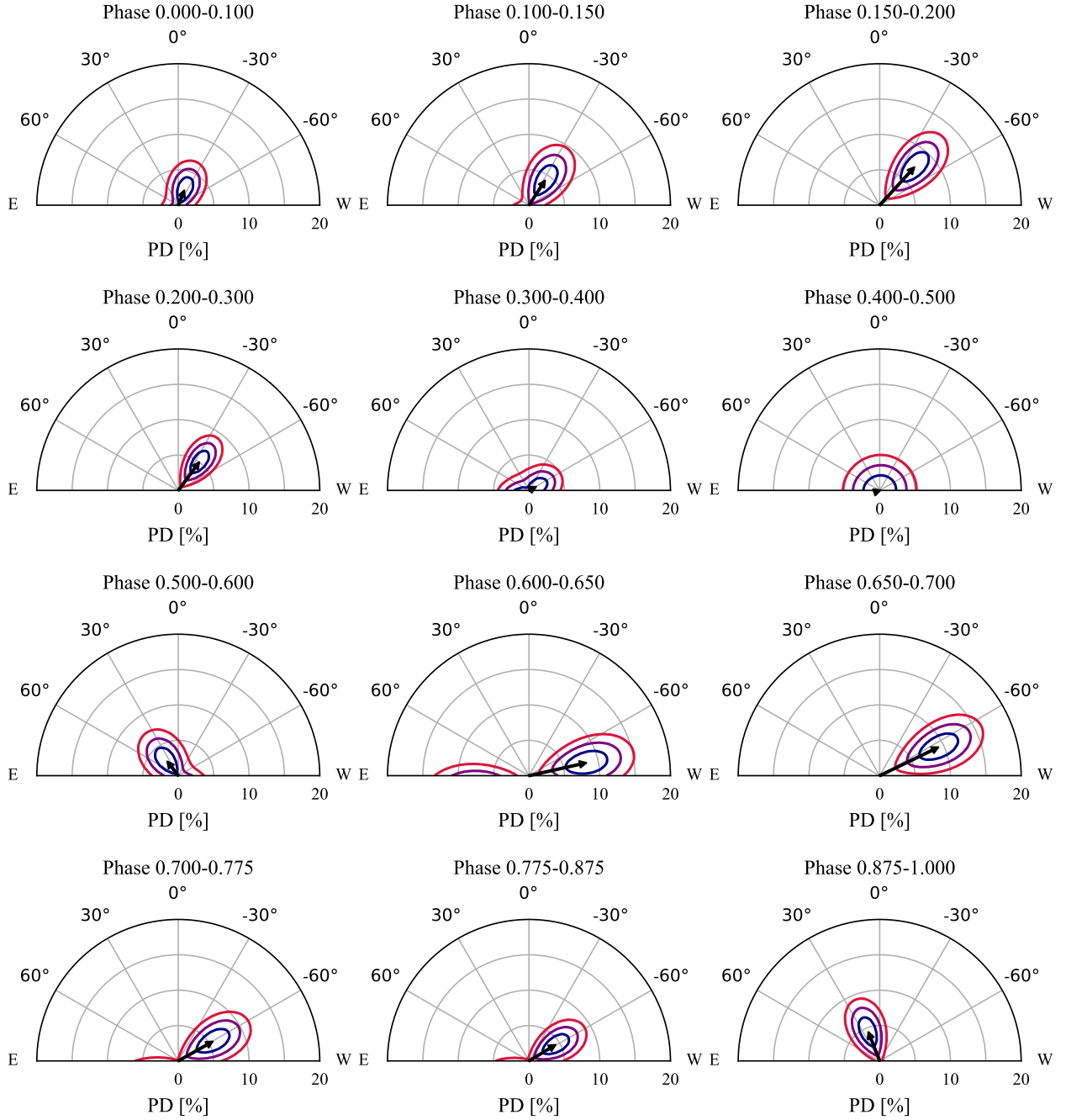


Figure 7. Polarization vectors of Vela X-1 from the results of the phase-resolved spectro-polarimetric analysis of the combined data set. Contours at 68.3%, 95.45% and 99.73% confidence, are shown in blue, purple, and red, respectively.

spectra were fitted with the same model as utilized for the phase-averaged spectro-polarimetric analysis, with the cross-calibration constants for DU2 and DU3 fixed to the values obtained for the phase-averaged analysis (see Table 4). The results of the phase-resolved spectro-polarimetric analysis are summarized in Table 3 and confidence contours corresponding to each phase bin are shown in Figure 7.

A spectro-polarimetric phase-averaged analysis done separately for the eclipse data did not find a significant polarization, with an upper limit to the PD of 25.1% at 99.73% confidence level. An intensity-resolved spectro-polarimetric analysis performed on the combined data did not reveal a significant difference in polarization properties between different luminosity levels.

4. DISCUSSION AND SUMMARY

XRPs are prime targets for X-ray polarimetric missions, where a high PD has been theoretically predicted because of the strong dependence of the primary radiation processes on the polarization of X-ray photons. The birefringence of highly magnetized plasma allows for the radiative transfer to be treated in terms of two normal polarization modes: the ordinary (“O”) and extraordinary (“X”) mode (Gnedin & Pavlov 1974). These two modes have different orientations in relation to the plane made up by the direction of the magnetic field and the momentum of photons. For O-mode photons, the electric vector oscillates mainly within the plane, while for X-mode photons the electric vector oscillations are mainly oriented perpendicular to the plane. Below the cyclotron energy the opacities of the polarization modes differ significantly, where the opacity of the X-mode is largely reduced compared to that of the O-mode (Lai & Ho 2003), resulting in the predictions for PD as high as 80% (Meszaros et al. 1988; Caiazzo & Heyl 2021).

However, a significantly lower PD of only $\sim 2.3\%$ detected for Vela X-1 in the IXPE data is in line with recent measurements done for other accreting XRPs (Her X-1, Doroshenko et al. 2022; Cen X-3, Tsygankov et al. 2022; 4U 1626–67, Marshall et al. 2022), where similar, relatively low PDs have been reported. The X-ray polarization of accreting XRPs greatly depends on the structure of the emission region (which is unknown), and most theoretical models mentioned here do not account yet for the temperature structure of the NS atmosphere, assuming instead a uniform temperature in the spectral forming region. In the case of the above-mentioned XRPs, the contradiction between the observed and the theoretically predicted values of the PD was explained with a model of the neutron star atmosphere overheated by the accretion process.

The key factor for the depolarized emission in this model is a conversion of modes at the so-called vacuum resonance. In strong magnetic fields, both the plasma and the vacuum are birefringent, where vacuum birefringence is a fundamental QED effect. Generally speaking, the two effects (plasma and vacuum birefringence) tend to work against each other, and at vacuum resonance they cancel out (Mészáros & Ventura 1978). This leads to a transformation of the normal modes of radiation and a loss of the linear polarization degree. The vacuum resonance occurs at a plasma density $\rho_V \approx 10^{-4} B_{12}^2 E_{\text{keV}}^2$ [g cm $^{-3}$] for a given photon energy E (in keV) and local magnetic field strength $B_{12} = B/10^{12}$ G. This may result in a much smaller PD than normally predicted when considering the specific temperature structure of the atmospheres of accreting NSs. Doroshenko et al.

(2022) have shown that a low PD of the X-ray radiation can be achieved if the point of vacuum resonance is located in an atmospheric transition layer with a strong temperature gradient. If the transition region is located at the border of the overheated upper atmospheric layer and the cooler underlying atmosphere, the low PD occurs as a result of the fast mode conversion (Gnedin et al. 1978). For the specific atmospheric thickness of ~ 3 g cm $^{-2}$, corresponding to the Thomson optical depth around unity, a PD of the order of 10% can be achieved (Doroshenko et al. 2022). As lower PDs than previously predicted seem to be a staple of sub-critical XRPs, theoretical models may well have to take into account the specific temperature structure of the NS atmosphere. On the other hand, the average observed luminosity for Vela X-1 is $\sim 4 \times 10^{35}$ erg s $^{-1}$, roughly two orders of magnitude lower than the observed luminosities of Her X-1 and Cen X-3. Thus, it is rather puzzling that this scenario suggests a similar thickness of the overheated layer for a much smaller accretion rate; however, the key quantity here may be the proton stopping depth (Zel’dovich & Shakura 1969; Nelson et al. 1993; Zane et al. 2000; González-Caniulef et al. 2019).

The low PD may also be a result of the strong variations of the PD and PA with energy (see Figure 3), considering the evident $\sim 90^\circ$ difference in the PA below and above 3.5 keV. However, a complete and detailed analysis of the complicated energy dependence of the polarization properties of Vela X-1 is out of the scope of this paper and is subject to future, more extensive work.

Finally, we can speculate that the observed small PD is a result of strong variations of the PA with the pulsar phase. The observed pulse profile has a very complicated shape, which is related either to the complex structure of the surface magnetic field, or to the presence of a number of different components (see Tsygankov et al. 2022, for discussion). The present photon statistics allowed us to obtain significant detection of polarization in 9 out of 12 phase bins, while to resolve the variations of the PA we likely needed many more bins.

The Imaging X-ray Polarimetry Explorer (IXPE) is a joint US and Italian mission. The US contribution is supported by the National Aeronautics and Space Administration (NASA) and led and managed by its Marshall Space Flight Center (MSFC), with industry partner Ball Aerospace (contract NNM15AA18C). The Italian contribution is supported by the Italian Space Agency (Agenzia Spaziale Italiana, ASI) through contract ASI-OHBI-2017-12-I.0, agreements ASI-INAF-2017-12-H0 and ASI-INFN-2017.13-H0, and its Space Science Data Center (SSDC) with agreements ASI-INAF-2022-14-HH.0 and ASI-INFN 2021-43-HH.0, and by the Istituto Nazionale di Astrofisica (INAF) and the Istituto Nazionale di Fisica Nucleare (INFN) in Italy. This research used data products provided by the IXPE Team (MSFC, SSCD, INAF, and INFN) and distributed with additional software tools by the High-Energy Astrophysics Science Archive Research Center (HEASARC), at NASA Goddard Space Flight Center (GSFC).

We acknowledge support from the RSF grant 19-12-00423 (SST), the Academy of Finland grants 333112, 349144, 349373, and 349906 (JP, SST), the German Academic Exchange Service (DAAD) travel grant 57525212 (VD, VFS), and the German Research Foundation (DFG) grant WE 1312/53-1 (VFS).

Facilities: IXPE, Swift (XRT and UVOT), NuSTAR

Software: astropy (Astropy Collaboration et al. 2013, 2018), XSPEC (Arnaud 1996), IXPEOBSSIM (Baldini et al. 2022).

REFERENCES

- Arnaud, K. A. 1996, in ASP Conf. Ser., Vol. 101, Astronomical Data Analysis Software and Systems V, ed. G. H. Jacoby & J. Barnes (San Francisco: Astron. Soc. Pac.), 17–20
- Astropy Collaboration, Robitaille, T. P., Tollerud, E. J., et al. 2013, *A&A*, 558, A33, doi: [10.1051/0004-6361/201322068](https://doi.org/10.1051/0004-6361/201322068)
- Astropy Collaboration, Price-Whelan, A. M., Sipőcz, B. M., et al. 2018, *AJ*, 156, 123, doi: [10.3847/1538-3881/aabc4f](https://doi.org/10.3847/1538-3881/aabc4f)
- Baldini, L., Bucciantini, N., Di Lalla, N., et al. 2022, *SoftwareX*, 19, 101194, doi: [10.1016/j.softx.2022.101194](https://doi.org/10.1016/j.softx.2022.101194)
- Caiazzo, I., & Heyl, J. 2021, *MNRAS*, 501, 109, doi: [10.1093/mnras/staa3428](https://doi.org/10.1093/mnras/staa3428)
- Chodil, G., Mark, H., Rodrigues, R., Seward, F. D., & Swift, C. D. 1967, *ApJ*, 150, 57, doi: [10.1086/149312](https://doi.org/10.1086/149312)
- Di Marco, A., Soffitta, P., Costa, E., et al. 2023, arXiv e-prints, arXiv:2302.02927, doi: [10.48550/arXiv.2302.02927](https://doi.org/10.48550/arXiv.2302.02927)
- Doroshenko, V., Poutanen, J., Tsygankov, S. S., et al. 2022, *Nature Astronomy*, 6, 1433, doi: [10.1038/s41550-022-01799-5](https://doi.org/10.1038/s41550-022-01799-5)
- Fürst, F., Pottschmidt, K., Wilms, J., et al. 2014, *ApJ*, 780, 133, doi: [10.1088/0004-637X/780/2/133](https://doi.org/10.1088/0004-637X/780/2/133)
- Gnedin, Y. N., & Pavlov, G. G. 1974, *Soviet Journal of Experimental and Theoretical Physics*, 38, 903
- Gnedin, Y. N., Pavlov, G. G., & Shibanov, Y. A. 1978, *Soviet Astronomy Letters*, 4, 117
- González-Caniulef, D., Zane, S., Turolla, R., & Wu, K. 2019, *MNRAS*, 483, 599, doi: [10.1093/mnras/sty3159](https://doi.org/10.1093/mnras/sty3159)

- Ji, L., Staubert, R., Ducci, L., et al. 2019, MNRAS, 484, 3797, doi: [10.1093/mnras/stz264](https://doi.org/10.1093/mnras/stz264)
- Kendziorra, E., Mony, B., Kretschmar, P., et al. 1992, in Proc. Yamada Conf. XXVIII, Frontiers Science Series, ed. Y. Tanaka & K. Koyama (Tokyo: Universal Academy Press), 51
- Kislat, F., Clark, B., Beilicke, M., & Krawczynski, H. 2015, Astroparticle Physics, 68, 45, doi: [10.1016/j.astropartphys.2015.02.007](https://doi.org/10.1016/j.astropartphys.2015.02.007)
- Kretschmar, P., Pan, H. C., Kendziorra, E., et al. 1996, A&AS, 120, 175
- . 1997, A&A, 325, 623
- Kretschmar, P., El Mellah, I., Martínez-Núñez, S., et al. 2021, A&A, 652, A95, doi: [10.1051/0004-6361/202040272](https://doi.org/10.1051/0004-6361/202040272)
- Kreykenbohm, I., Wilms, J., Kretschmar, P., et al. 2008, A&A, 492, 511, doi: [10.1051/0004-6361:200809956](https://doi.org/10.1051/0004-6361:200809956)
- La Parola, V., Cusumano, G., Segreto, A., & D’Ai, A. 2016, MNRAS, 463, 185, doi: [10.1093/mnras/stw1915](https://doi.org/10.1093/mnras/stw1915)
- Lai, D., & Ho, W. C. 2003, PhRvL, 91, 071101, doi: [10.1103/PhysRevLett.91.071101](https://doi.org/10.1103/PhysRevLett.91.071101)
- Maier, D., Tenzer, C., & Santangelo, A. 2014, PASP, 126, 459, doi: [10.1086/676820](https://doi.org/10.1086/676820)
- Makishima, K., & Mihara, T. 1992, in Proc. Yamada Conf. XXVIII, Frontiers Science Series, ed. Y. Tanaka & K. Koyama (Tokyo: Universal Academy Press), 23
- Marshall, H. L., Ng, M., Rogantini, D., et al. 2022, ApJ, 940, 70, doi: [10.3847/1538-4357/ac98c2](https://doi.org/10.3847/1538-4357/ac98c2)
- McClintock, J. E., Rappaport, S., Joss, P. C., et al. 1976, ApJL, 206, L99, doi: [10.1086/182142](https://doi.org/10.1086/182142)
- Meszáros, P., Novick, R., Szentgyorgyi, A., Chanan, G. A., & Weisskopf, M. C. 1988, ApJ, 324, 1056, doi: [10.1086/165962](https://doi.org/10.1086/165962)
- Mészáros, P., & Ventura, J. 1978, PhRvL, 41, 1544, doi: [10.1103/PhysRevLett.41.1544](https://doi.org/10.1103/PhysRevLett.41.1544)
- Mikhalev, V. 2018, A&A, 615, A54, doi: [10.1051/0004-6361/201731971](https://doi.org/10.1051/0004-6361/201731971)
- Mushtukov, A., & Tsygankov, S. 2022, arXiv e-prints, arXiv:2204.14185. <https://arxiv.org/abs/2204.14185>
- Nagase, F., Hayakawa, S., Sato, N., Masai, K., & Inoue, H. 1986, PASJ, 38, 547
- Nelson, R. W., Salpeter, E. E., & Wasserman, I. 1993, ApJ, 418, 874, doi: [10.1086/173445](https://doi.org/10.1086/173445)
- Quaintrell, H., Norton, A. J., Ash, T. D. C., et al. 2003, A&A, 401, 313, doi: [10.1051/0004-6361:20030120](https://doi.org/10.1051/0004-6361:20030120)
- Serkowski, K. 1958, AcA, 8, 135
- Simmons, J. F. L., & Stewart, B. G. 1985, A&A, 142, 100
- Soffitta, P., Baldini, L., Bellazzini, R., et al. 2021, AJ, 162, 208, doi: [10.3847/1538-3881/ac19b0](https://doi.org/10.3847/1538-3881/ac19b0)
- Staubert, R., Kreykenbohm, I., Kretschmar, P., et al. 2004, in ESA Spec. Publ., Vol. 552, 5th INTEGRAL Workshop, the INTEGRAL Universe, ed. V. Schoenfelder, G. Lichti, & C. Winkler, 259
- Tsygankov, S. S., Doroshenko, V., Poutanen, J., et al. 2022, ApJL, 941, L14, doi: [10.3847/2041-8213/aca486](https://doi.org/10.3847/2041-8213/aca486)
- Ulmer, M. P., Baity, W. A., Wheaton, W. A., & Peterson, L. E. 1972, ApJL, 178, L121, doi: [10.1086/181099](https://doi.org/10.1086/181099)
- van Kerkwijk, M. H., van Paradijs, J., Zuiderwijk, E. J., et al. 1995, A&A, 303, 483. <https://arxiv.org/abs/astro-ph/9505070>
- Weisskopf, M. C., Elsner, R. F., & O’Dell, S. L. 2010, in Proc. SPIE, Vol. 7732, Space Telescopes and Instrumentation 2010: Ultraviolet to Gamma Ray, ed. M. Arnaud, S. S. Murray, & T. Takahashi, 77320E, doi: [10.1117/12.857357](https://doi.org/10.1117/12.857357)
- Weisskopf, M. C., Soffitta, P., Baldini, L., et al. 2022, J. Astron. Telesc. Instrum. Syst., 8, 026002, doi: [10.1117/1.JATIS.8.2.026002](https://doi.org/10.1117/1.JATIS.8.2.026002)
- Wilms, J., Allen, A., & McCray, R. 2000, ApJ, 542, 914, doi: [10.1086/317016](https://doi.org/10.1086/317016)
- Zane, S., Turolla, R., & Treves, A. 2000, ApJ, 537, 387, doi: [10.1086/309027](https://doi.org/10.1086/309027)
- Zel’dovich, Y. B., & Shakura, N. I. 1969, Soviet Ast., 13, 175